Supplement of Biogeosciences, 22, 1509–1528, 2025
https://doi.org/10.5194/bg-22-1509-2025-supplement

Biogeosciences Open Access EGU

Supplement of

Constraining 2010–2020 Amazonian carbon flux estimates with satellite solar-induced fluorescence (SIF)

Archana Dayalu et al.

Correspondence to: Archana Dayalu (adayalu@aer.com)

Supplementary Information

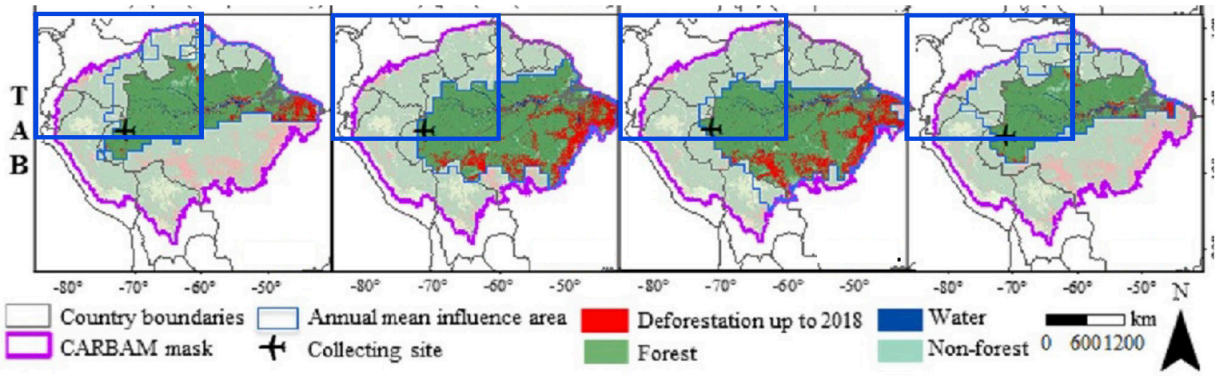

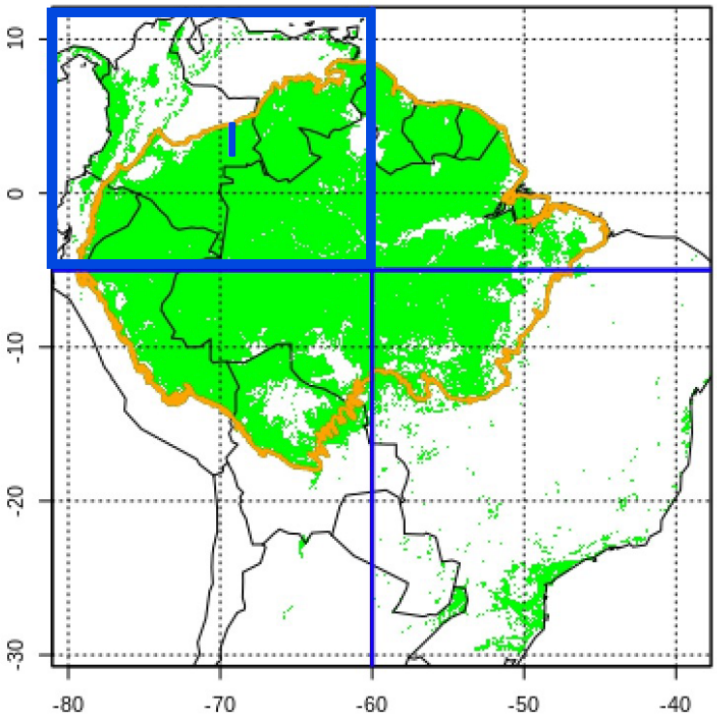

Figure S1. **Special treatment of evergreen broadleaf class in Amazon basin.** (Top) Figure adapted from Gatti et al. (2021) showing deforestation extent through 2018 (red). Deforestation in interior/western Amazon basin (blue quadrant) is significantly less. (Bottom) EBLF classes in blue quadrant calibrated with K34 Interior Amazon eddy flux measurements to reflect carbon exchange in a more ecologically intact rainforest.

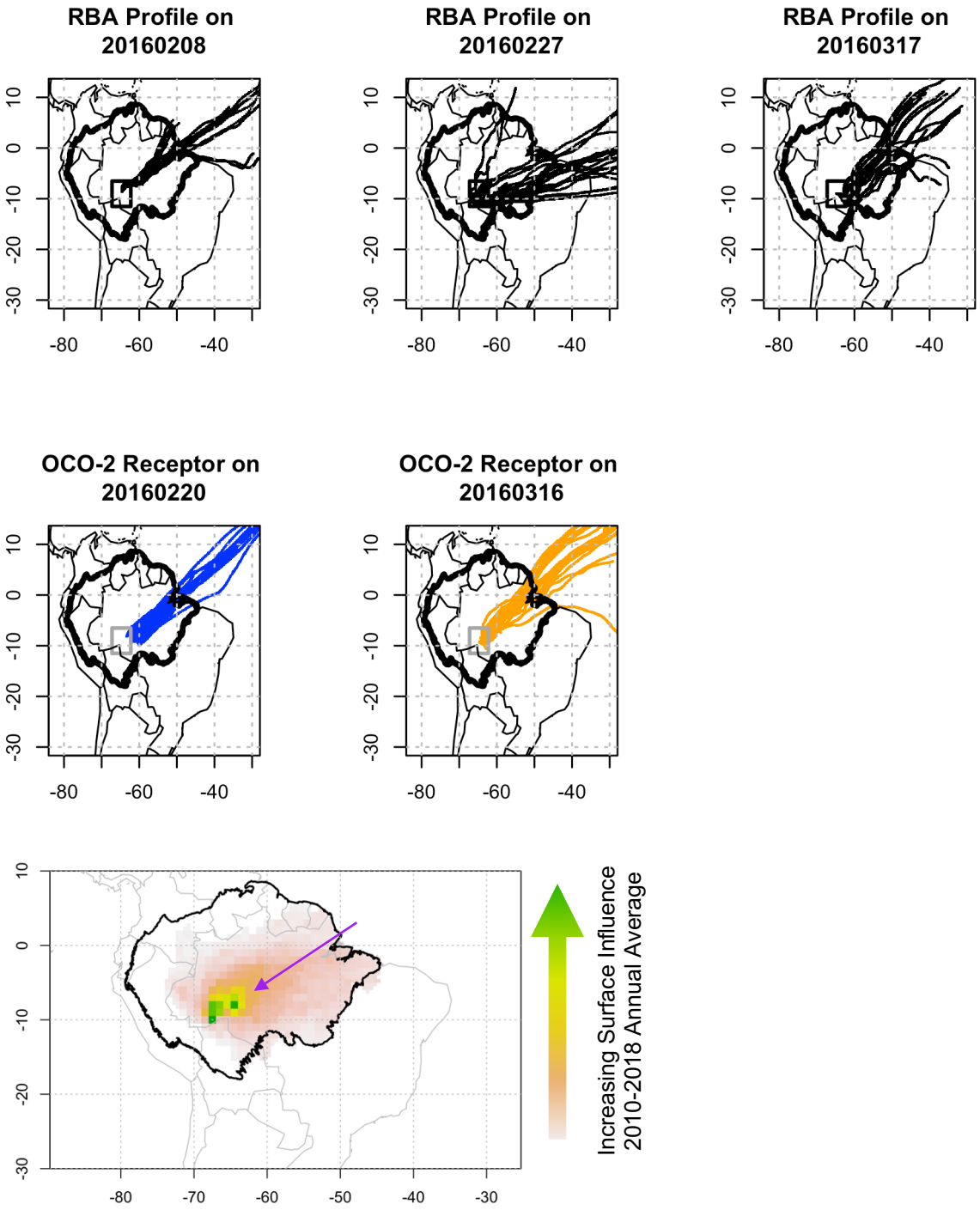

Figure S2. NOAA HYSPLIT 10-day back trajectories in 5x5degree bounding box surrounding RBA, representing influences for a typical 2016 wet season month. (Top Row) Back trajectories corresponding to dates, times, and locations of actual aircraft vertical profiles. (Middle Row) Back trajectories corresponding to dates, times, and location of available and representative OCO-2 receptors. (Bottom Row) Weighted annual influences (2010 to 2018) from Gatti et al. (2021) generally track prevailing wet season 2016 wind direction.

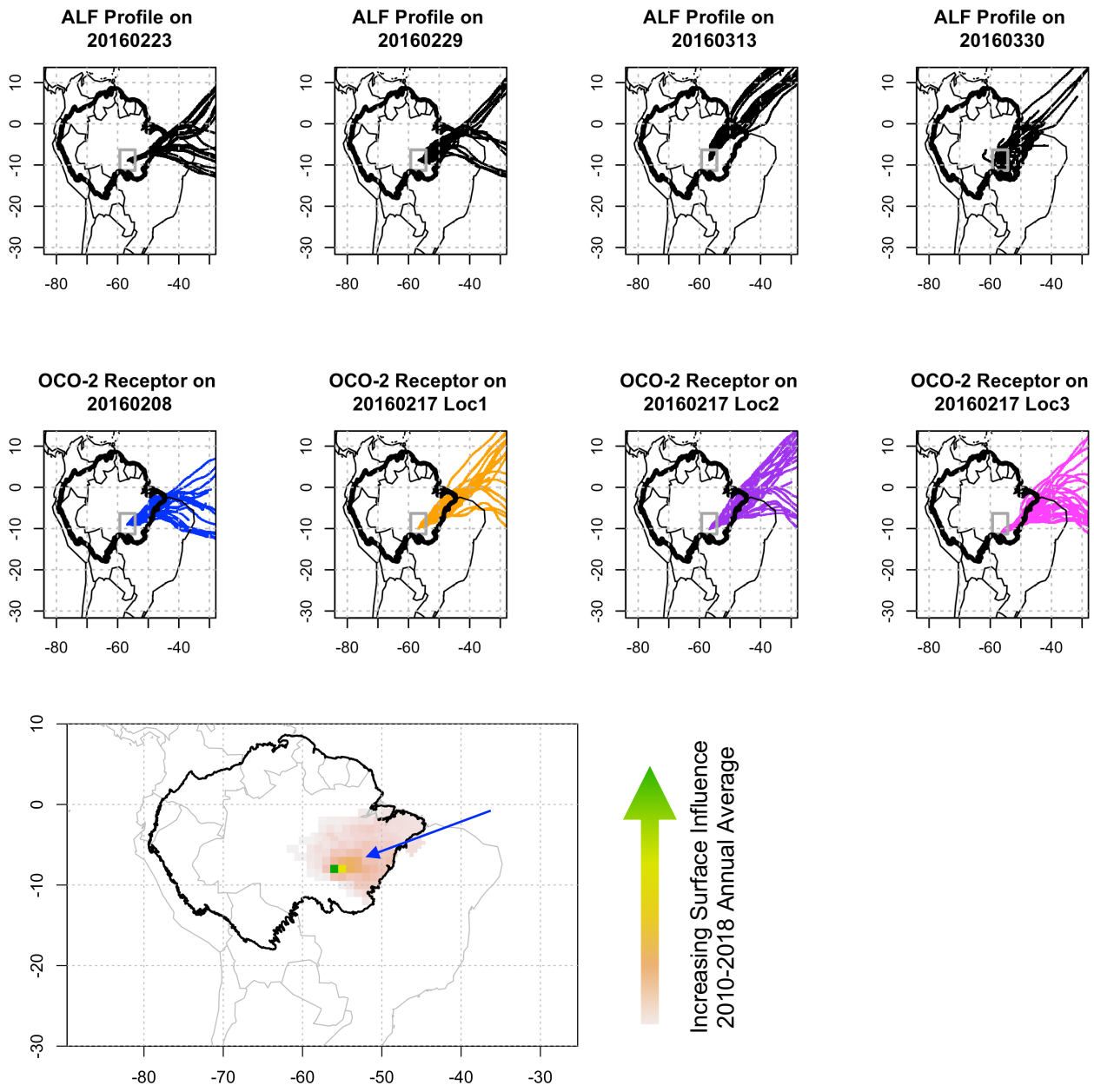

Figure S3. NOAA HYSPLIT 10-day back trajectories in 5x5degree bounding box surrounding ALF, representing influences for a typical 2016 wet season month. (Top Row) Back trajectories corresponding to dates, times, and locations of actual aircraft vertical profiles. (Bottom Row) Back trajectories corresponding to dates, times, and location of available and representative OCO-2 receptors. (Bottom Row) Weighted annual influences (2010 to 2018) from Gatti et al. (2021) generally track prevailing wet season 2016 wind direction.

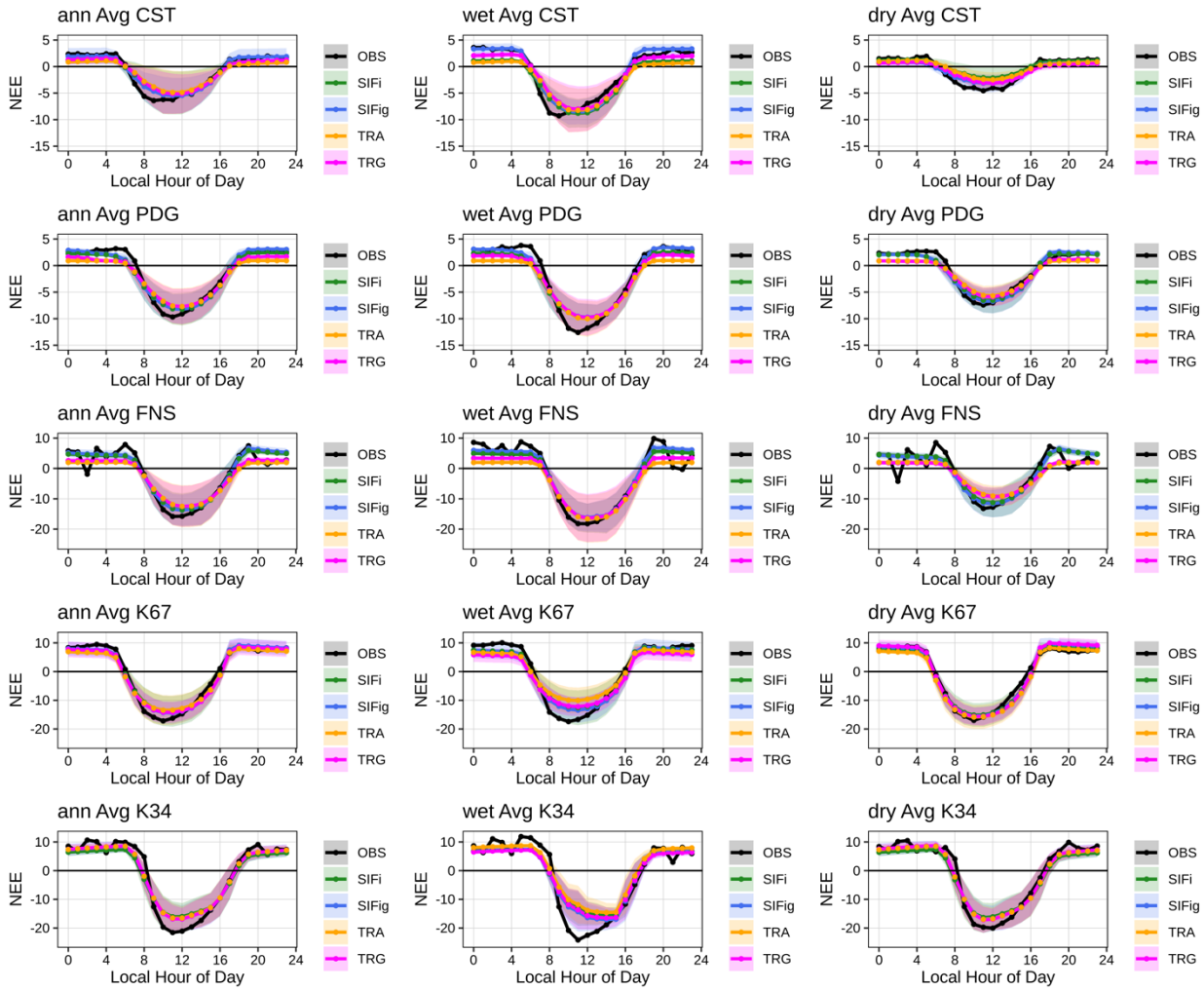

Figure S4. Diurnal results, calibration sites.

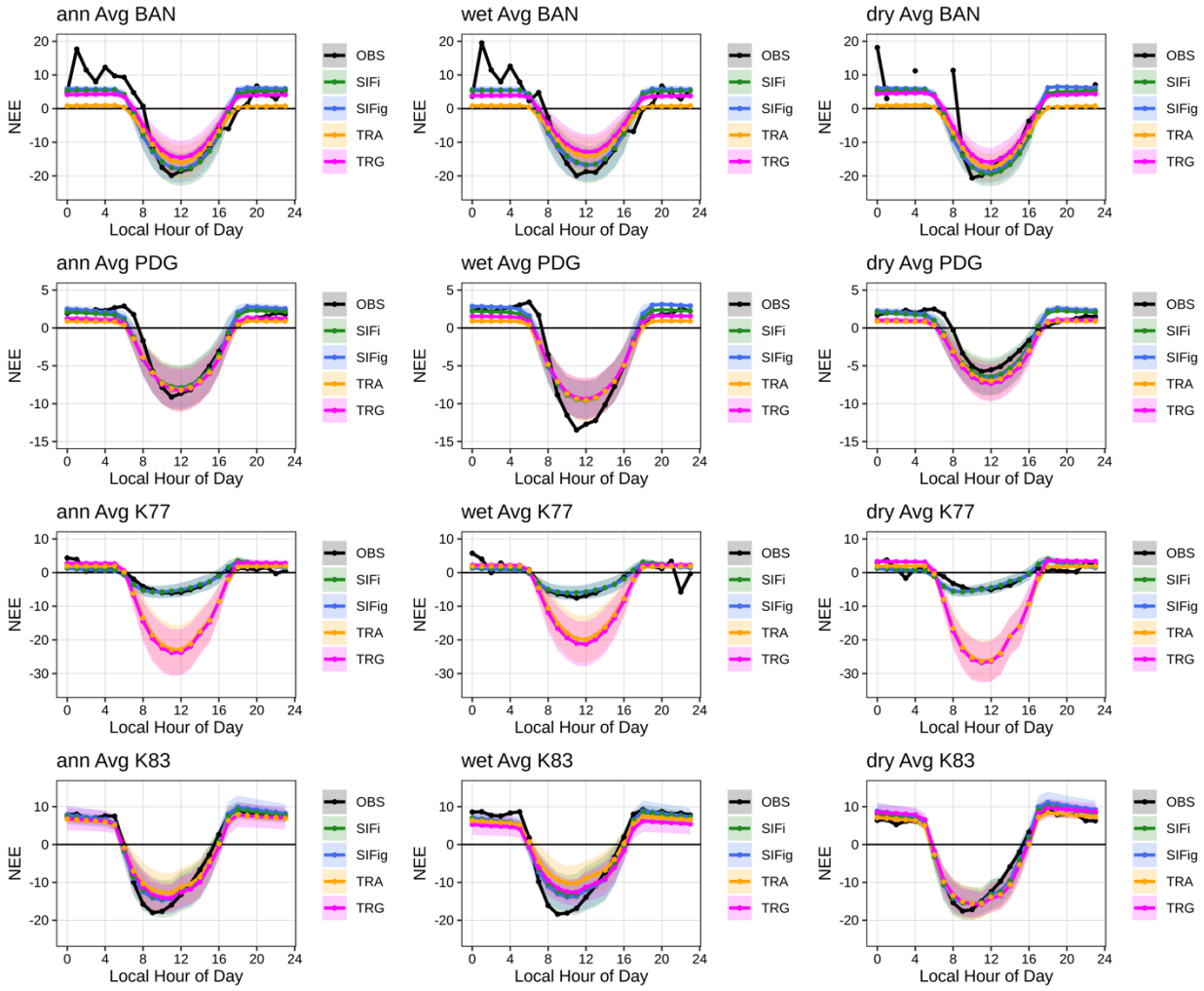

Figure S5. Diurnal results, validation sites.

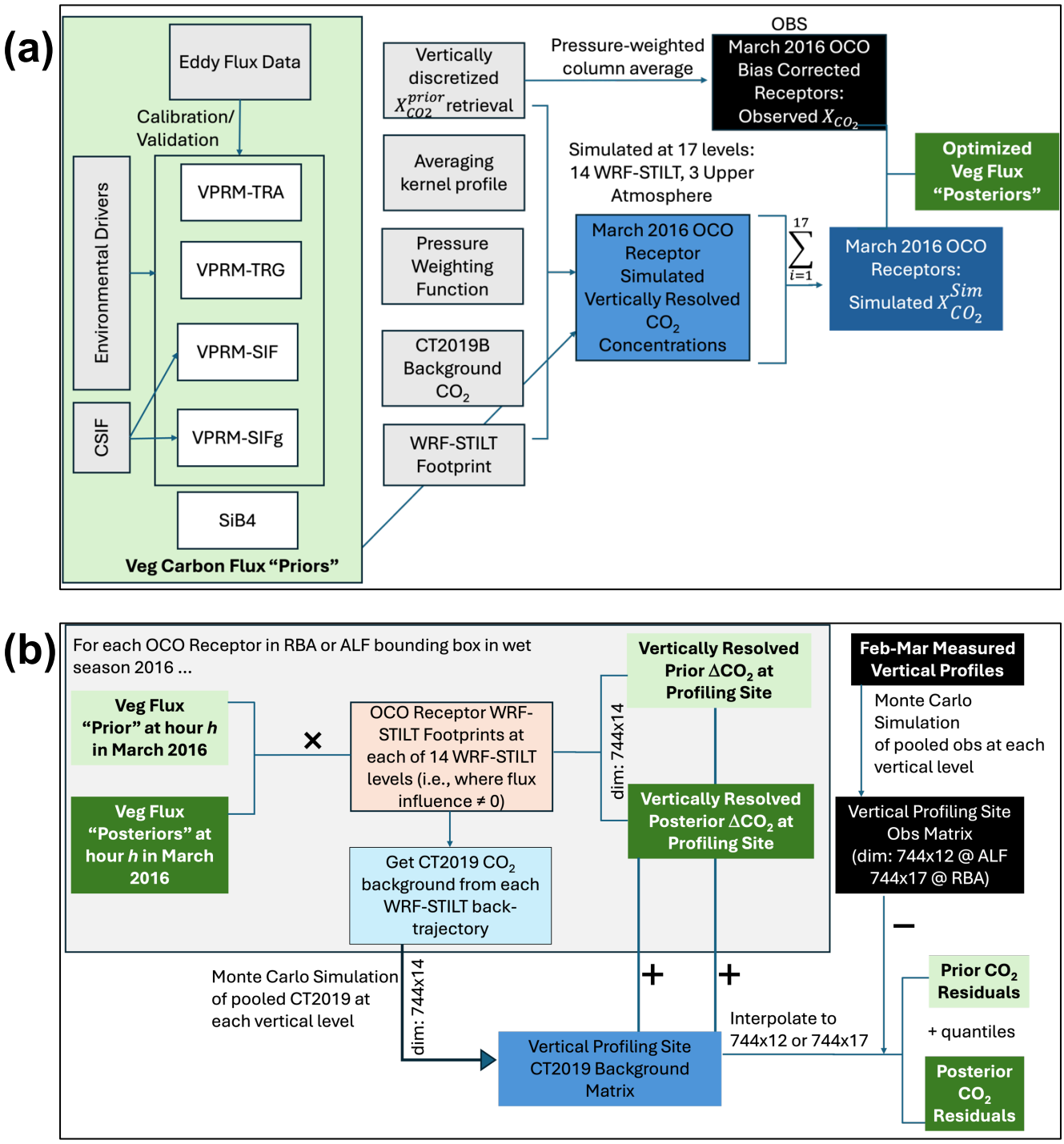

Figure S6. Flowchart of methodology. (a) Overall methodology; (b) aircraft vertical profile site simulation and comparison.

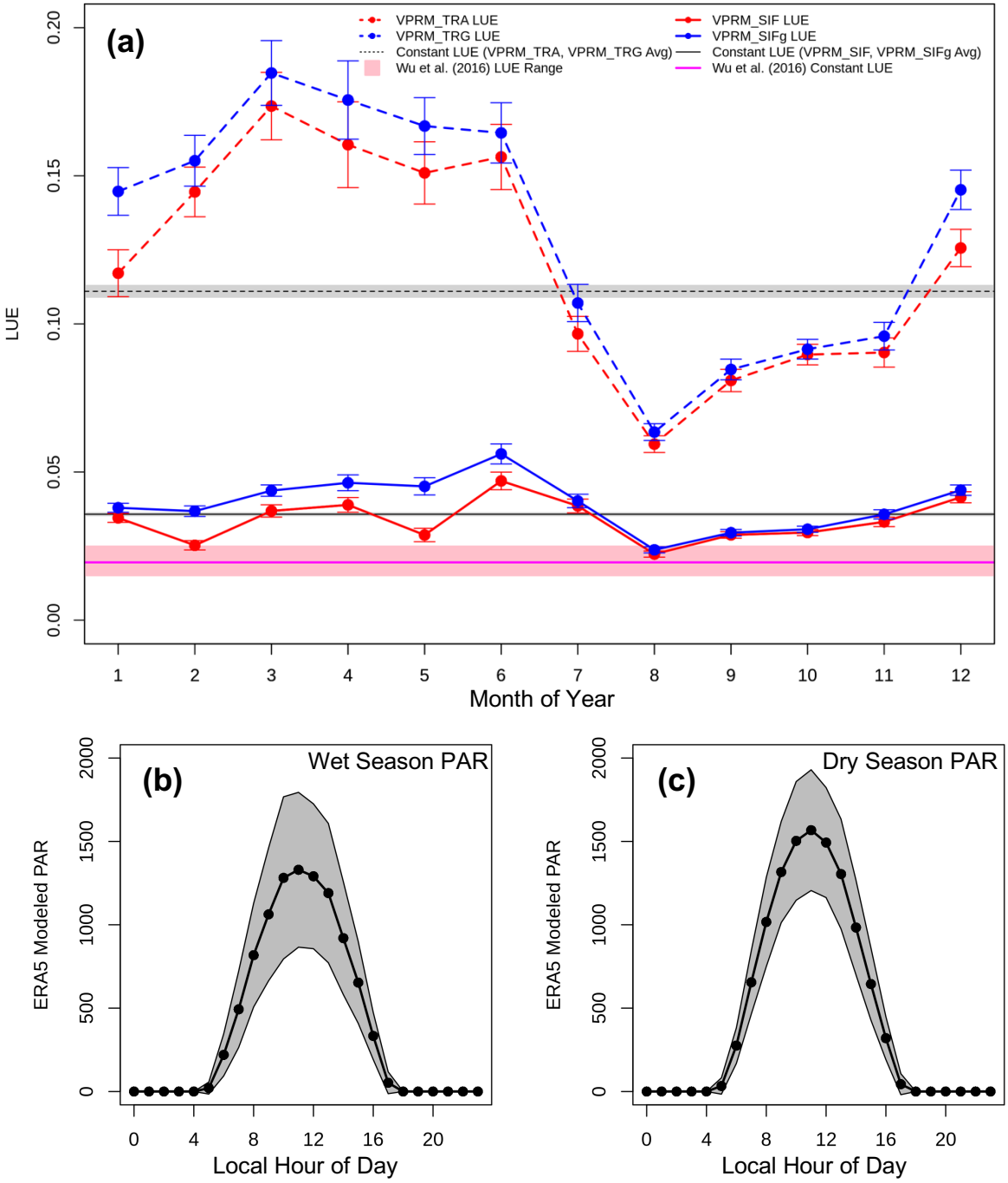

Figure S7. Light Use Efficiency and ERA5 modeled PAR at Br-K67. (a) Monthly and constant LUE estimated by VPRM and Wu et al. (2017). Note that error bars are 1-σ standard deviation from NLS parameter fitting; (b) modelled PAR.

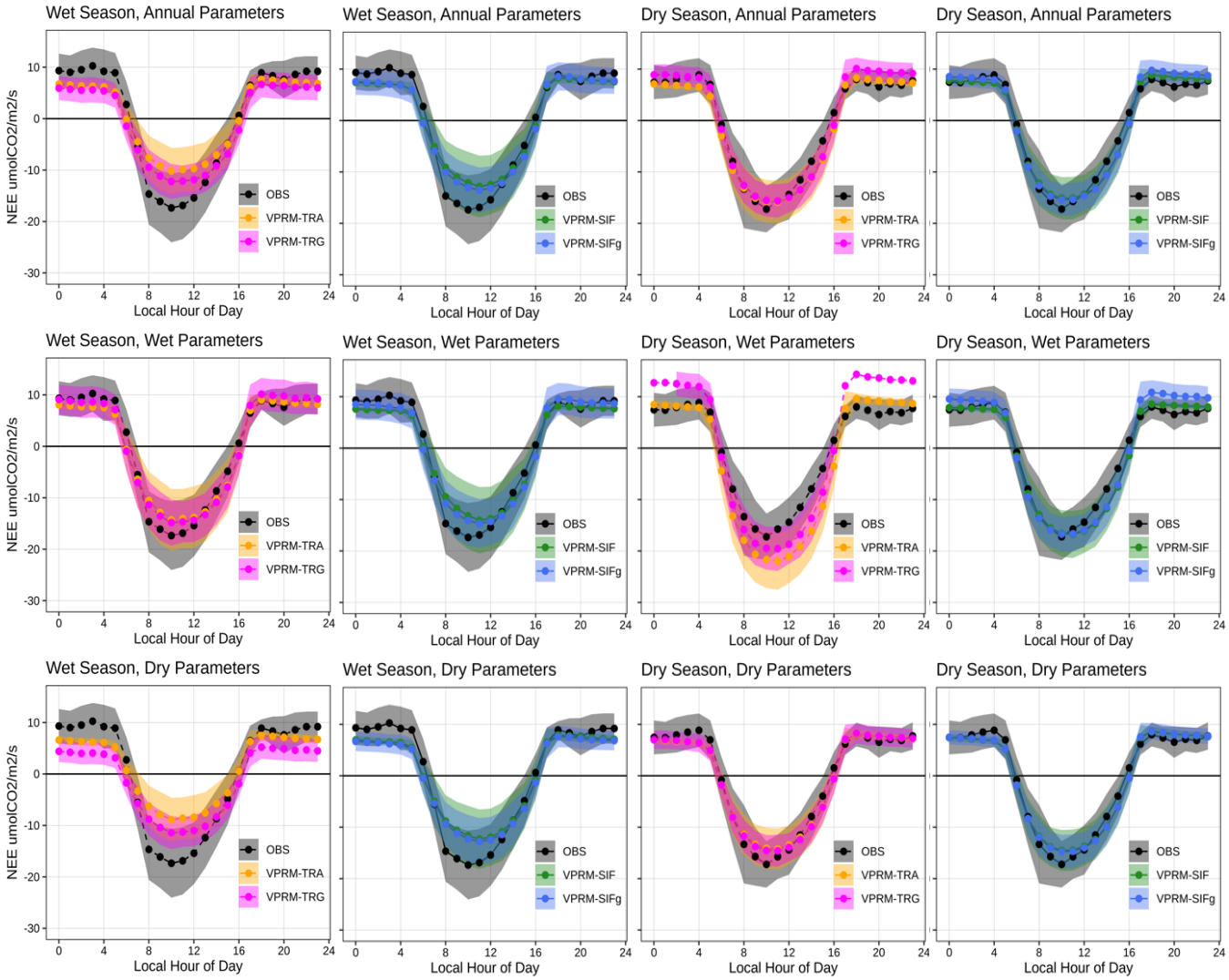

Figure S8. Seasonal fits to Br-K67 and diurnal model performance. Left panels: wet season; right panels: dry season.

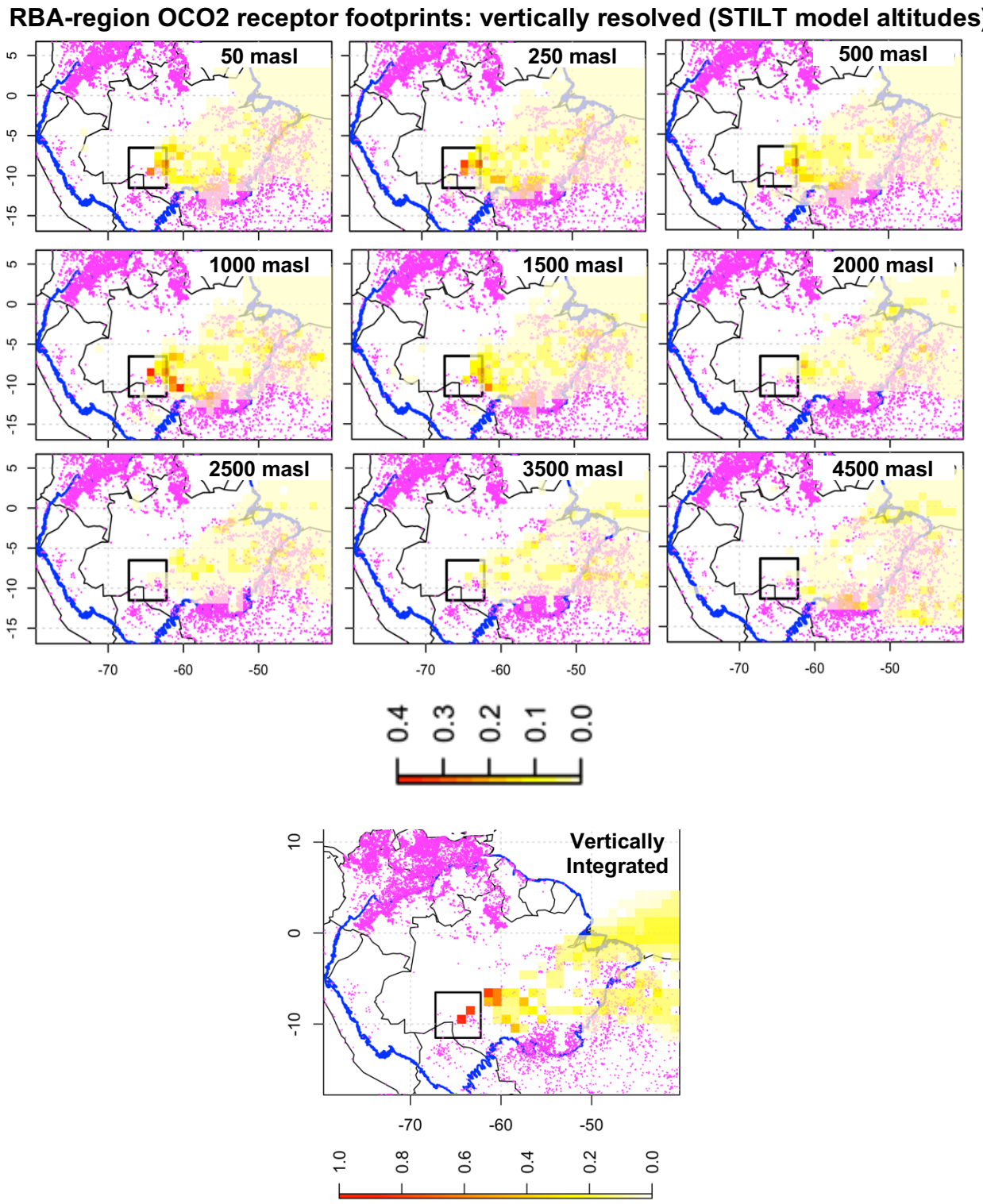

Figure S9. Vertically resolved footprints at RBA used in vertical profile simulation. Magenta points are fire locations identified between February and March 2016.

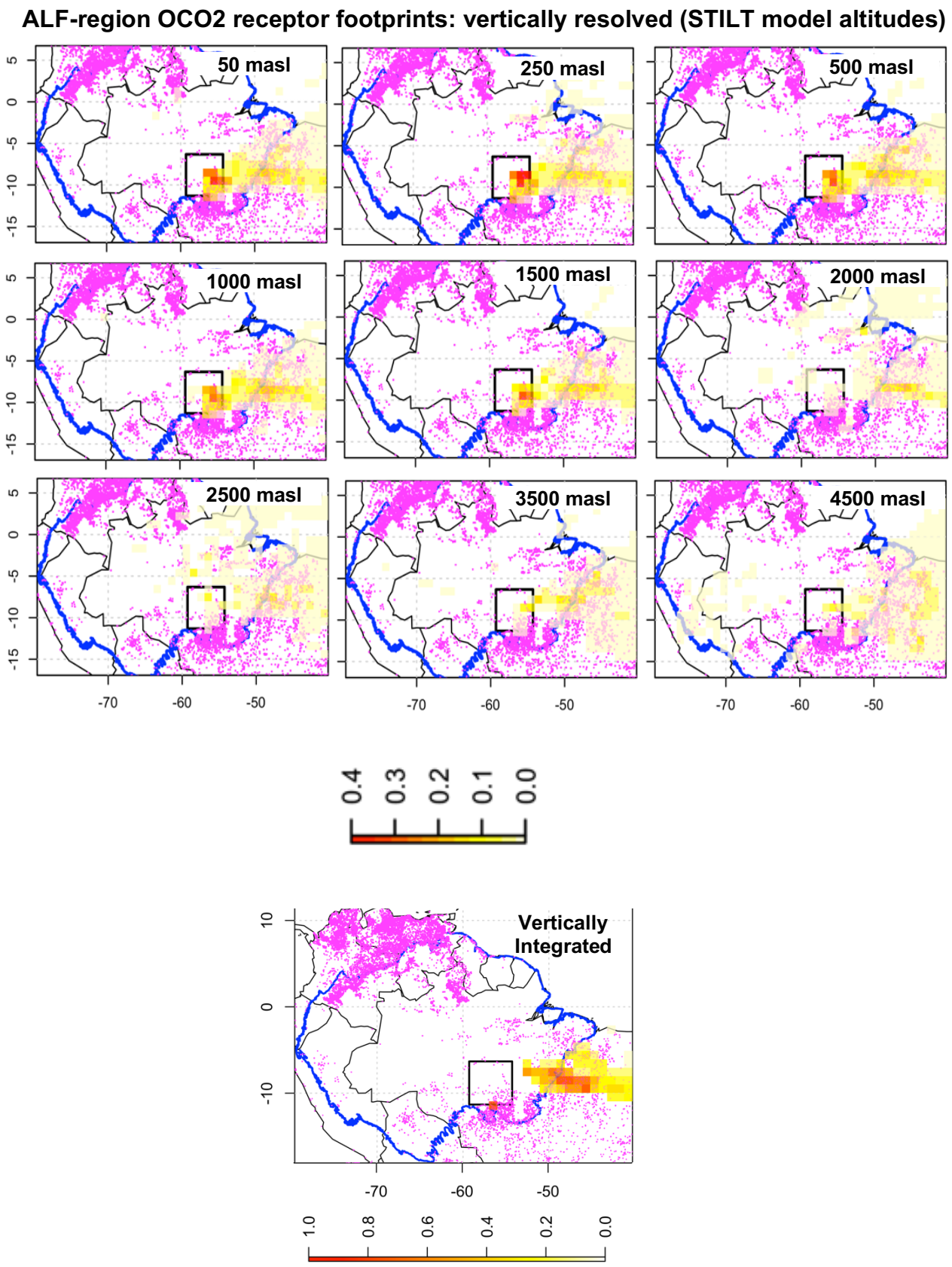

Figure S10. Vertically resolved footprints at ALF used in vertical profile simulation. Magenta points are fire locations identified between February and March 2016.

Table S1. **WRFv3.8.1 model configuration details**.

Option	Description
Land-surface	Noah land-surface model with MM5 Monin-Obukov surface layer
PBL package	Yongsei University (YSU) scheme
LW radiation	RRTMG
SW radiation	RRTMG
Microphysics	Lin et al.
Convection	Grell-Freitas
Nesting	One-way
Nudging	u,v,T,q at all levels above PBL in d01; u,v in PBL in d01; every 6 h; 1 h relaxation time
Time stepping	3rd order Runge-Kutta; 4 short time steps per long time step
Advection	5th order horizontal, 3rd order vertical positive definite advection for moisture and scalars
Diffusion	2nd order horizontal diffusion using Smagorinsky first-order closure
Damping	No upper level or vertical velocity damping; default values for divergence and external model damping

Table S2. Calibration parameters for ecosystem classes represented by eddy flux sites in VPRM domain. Values and standard deviation provided for each parameter from NLS fitting to non-gapfilled observational data. VPRM model version shown as one of TRA, TRG, SIF, SIFg. For Br-K67, results from seasonal fitting are also provided, as blue font (wet season) and brown font (dry season).

		Eddy Flux Site Used in VPRM Calibration				
		Br-CST	**Br-FNS**	**Br-K34**	**Br-K67**	**Br-PDG**
λ (σ)	**TRA**	0.047 (0.00)	0.067 (0.01)	0.052 (0.01)	0.106 (0.00) 0.138 (0.00) 0.087 (0.00)	0.037 (0.00)
	TRG	0.067 (0.01)	0.082 (0.01)	0.051 (0.01)	0.116 (0.00) 0.160 (0.00) 0.088 (0.00)	0.044 (0.00)
	SIF	0.019 (0.00)	0.029 (0.00)	0.024 (0.00)	0.034 (0.00) 0.033 (0.00) 0.032 (0.00)	0.016 (0.00)
	SIFg	0.033 (0.00)	0.032 (0.00)	0.023 (0.00)	0.038 (0.00) 0.041 (0.00) 0.032 (0.00)	0.019 (0.00)
PAR_0 (σ)	**TRA**	4608 (1380)	2427 (628)	1818 (489)	733 (21) 731 (30) 886 (29)	1996 (328)
	TRG	2377 (434)	1841 (405)	1994 (542)	701 (17) 655 (23) 900 (28)	1572 (238)
	SIF	2295 (379)	1256 (127)	1443 (351)	802 (18) 888 (40) 854 (30)	1296 (151)
	SIFg	1085 (109)	1118 (107)	1675 (405)	745 (15) 747 (27) 863 (29)	1058 (122)
α (σ)	**TRA**	-0.095 (0.02)	-0.050 (0.05)	-0.820 (0.07)	0.678 (0.03) 0.688 (0.03) 0.644 (0.04)	0.015 (0.02)
	TRG	-0.095 (0.02)	0.082 (0.06)	-0.823 (0.07)	0.586 (0.02) 0.823 (0.04) 0.629 (0.03)	0.035 (0.02)
	SIF	-0.0519 (0.02)	0.504 (0.05)	-0.693 (0.07)	0.616 (0.02) 0.409 (0.04) 0.677 (0.03)	0.107 (0.02)
	SIFg	-0.023 (0.01)	0.634 (0.05)	-0.792 (0.06)	0.709 (0.02) 0.737 (0.04) 0.673 (0.03)	0.134 (0.02)
β (σ)	**TRA**	3.15 (0.42)	3.10 (1.3)	28.0 (2.0)	-10.0 (0.64) -8.92 (1.1) -9.29 (0.71)	0.571 (0.42)
	TRG	0.179 (0.45)	-5.96 (2.6)	9.13 (4.1)	-20.8 (0.62) -25.8 (1.1) -21.6 (0.77)	-2.87 (0.89)
	SIF	2.37 (0.39)	-6.72 (1.1)	23.7 (1.8)	-7.74 (0.53) -2.47 (1.1) -9.70 (0.79)	-0.290 (0.42)
	SIFg	-0.092 (0.37)	-13.2 (1.8)	5.41 (2.7)	-21.6 (0.55) -23.3 (1.1) -17.8 (0.88)	-2.07 (0.63)
γ (σ)	**TRA**	--	--	--	--	--
	TRG	14.5 (0.91)	14.3 (3.6)	37.1 (7.1)	29.0 (0.49) 34.6 (0.88) 24.7 (0.72)	7.62 (1.7)
	SIF	--	--	--	--	--
	SIFg	7.33 (0.28)	3.05 (0.67)	18.4 (2.1)	8.59 (0.15) 10.0 (0.22) 5.79 (0.31)	1.71 (0.45)

Table S3. Respiration bias by ecosystem type. Italicized font is used for validation sites. Bold values indicate overestimate of respiration relative to observations; normal font is underestimated relative to observations.

Respiration Bias			Median Model-Obs Bias (μmol $CO_2/m_2/s$)			
Site	**IGBP**	**Season**	**TRA**	**TRG**	**SIF**	**SIFg**
Br-BAN	*Woody Sav*	*Ann*	*-3.5*	*-1.1*	*-0.20*	***0.82***
		Wet	*-3.2*	*-0.94*	*-0.17*	***0.83***
		Dry	*-6.0*	*-2.5*	*-1.5*	*-1.3*
Br-CST	Woody Sav	Ann	-0.47	-0.57	-0.16	-0.19
		Wet	-1.8	-0.60	-1.4	**0.64**
		Dry	-0.058	-0.56	**0.23**	-0.46
Br-K77	*Grasslands*	*Ann*	***0.36***	***0.93***	*-0.047*	*-0.45*
		Wet	*-0.74*	*-0.20*	*-0.82*	*-0.98*
		Dry	***0.78***	***2.1***	***0.71***	***0.50***
Br-FNS	Grasslands	Ann	-3.1	-3.2	-0.80	-0.43
		Wet	-4.8	-3.6	-1.8	-0.64
		Dry	-2.5	-2.8	-0.13	-0.11
Br-PDGa	*Savannas*	*Ann*	*-0.16*	***0.17***	***1.1***	***1.5***
		Wet	*-0.23*	***0.57***	***1.1***	***1.9***
		Dry	*-0.13*	***0.078***	***1.1***	***1.3***
Br-PDGb	Savannas	Ann	-0.96	-0.43	**0.51**	**0.92**
		Wet	-2.0	-1.1	**0.42**	**0.48**
		Dry	-0.54	-0.32	**0.88**	**1.0**
Br-K83	*Evergreen Bdlf*	*Ann*	*-1.4*	*-1.5*	*-0.86*	*-0.22*
		Wet	*-2.3*	*-3.4*	*-1.9*	*-1.4*
		Dry	***0.55***	***2.3***	***1.4***	***2.7***
Br-K67	Evergreen Bdlf	Ann	-1.4	-0.39	-1.0	**0.019**
		Wet	-2.8	-3.7	-2.1	-1.3
		Dry	-0.17	**2.4**	**0.54**	**1.8**
Br-K34	Evergreen Bdlf	Ann	-1.2	-1.1	-1.6	-2.1
		Wet	-3.9	-4.6	-4.8	-4.5
		Dry	-1.2	-0.61	-1.5	-1.1

S1 Impact of Seasonality on VPRM Performance: Br-K67

Wu et al. (2017) explore causes of GPP variability in Amazonian rainforests, focusing on the relative importance of light versus water limitations at the Br-K67 site, using data spanning 2002–2011. Wu et al. (2017) estimate monthly and constant light use efficiency (LUE; CO_2 uptake per unit of PAR) directly from the ratio of observationally derived GPP to PAR under reference (i.e., "non-stressed") environmental conditions. Their resulting reference monthly LUE ranges from 0.02 to 0.03 μmol CO_2 (μmol photons)$^{-1}$ over the seven years of Br-K67 eddy flux data in contrast to a constant LUE of ~0.02 μmol CO_2 (μmol photons)$^{-1}$. Wu et al. (2017) show seasonality in monthly LUE, with peak dry season values lower than peak wet season by as much as 33%. In this section, we present our results examining (1) seasonal variations in the LUE (i.e, the λ term in VPRM) term across model versions and compared to literature values; and (2) impacts of seasonality in VPRM fitting parameters on modelled relative to observed NEE both in aggregate and diurnally.

Figure S7a displays the monthly average LUE obtained from VPRM NLS fitting to all available Br-K67 data, with LUE estimated by Wu et al. (2017) included for reference. We note that all versions of the VPRM indicate a seasonal cycle in LUE whose timing is similar to Wu et al. (2017). However, while the traditional VPRM formulations estimate a peak dry season LUE that is 66% lower than the peak wet season LUE, the difference in SIF-based formulations is 39–46% lower in the dry season. The traditional VPRM versions estimate monthly LUE that is frequently an order of magnitude higher than those estimated by the SIF-based versions and in Wu et al. (2017). In contrast, both SIF-based VPRM formulations estimate LUE that is generally higher but comparable to Wu et al. (2017); differences are ascribed to the LUE estimation methodology. Overall, the LUE from SIF-based VPRM formulations have significantly better agreement with Wu et al. (2017); given the direct relation between LUE and GPP, our results provide higher confidence in SIF-based GPP estimates over the traditional VPRM GPP estimates. Seasonal variations in diurnally averaged modeled PAR are shown in Fig. S7b-c.

Given the seasonality in tropical forest LUE, and their dominance in domain land cover type, we next test our assumption that (1) the direct VPRM variables (i.e., SIF, Tscale, Pscale, EVI, LSWI, T_{air}) explain more of the real-time variation in carbon flux than the tuning parameters, and (2) constant annual-based tuning parameters can reasonably be used across seasons and years. Wu et al. (2017) have previously shown that while environmental drivers indeed explain the most variability at shorter (hourly) timescales, they tend to explain progressively less at longer timescales (diurnal, monthly, annual) when the influence from intrinsic ecosystem variables begin to aggregate. However, Wu et al. (2017) use an LUE-based photosynthesis model that is adopted from the VPRM-TRA formulation as in Mahadevan et al. (2008).

Table S4 summarizes the results from a test where the wet and dry season Br-K67 evaluation subsets (described in Sect. 2.2.2) were used to predict seasonal NEE from annual- and seasonal-fit calibration parameters (Table S2). Overall, while all models generally underestimated net uptake in the wet season and underestimated net release in the dry season, the VPRM-SIFg formulation performed consistently better across all calibration parameters with hourly errors ranging from 0-10%. As expected, the optimal model-observation fit across all model versions occurred when season-specific parameters were used (% error < 3). However, when seasonal NEE was predicted using calibration parameters tuned to the opposite season, VPRM-TRA performed the worst (% error: 53–71), followed by VPRM-

TRG (% error: 8.7–23), VPRM-SIF (% error: 11–18) and VPRM-SIFg (% error: 8.9–9.2). Finally, errors in seasonal NEE predictions from annual parameters smoothed the impacts of lower cross-season predictability; however, even with the cross-seasonal smoothing, the VPRM-TRA performed relatively poorly (% error: 19–36%), particularly when compared to VPRM-SIFg (% error: 2.7–6.9).

Table S4. Impact of calibration parameter seasonality on NEE predictability. Calibration parameters used in evaluation are obtained from the annual set where NLS fitting was conducted for entire Br-K67 data set (NEE_{ann}), the wet season where calibration was conducted for a random 70% subset of Br-K67 wet season data (NEE_{wet}), and the dry season where calibration was conducted for a random 70% subset of Br-K67 dry season data (NEE_{dry}). Mean Bias is reported for each of wet and dry seasons relative to hourly NEE observations in the 30% seasonal evaluation subsets. % Error (model relative to observations) and R^2 values are provided in parentheses.

		Mean Bias, µmol CO_2 m^{-2} s^{-1} (% error, R^2)	
Model	**Calibration Parameters**	**$NEE_{wet,VPRM}$ vs. $NEE_{wet,Obs}$**	**$NEE_{dry,VPRM}$ vs. $NEE_{dry,Obs}$**
VPRM-TRA	**NEE_{ann}**	1.92 (36.4, *0.72*)	-1.21 (18.9, *0.74*)
	NEE_{wet}	0.041 (0.788, *0.72*)	-4.54 (70.9, *0.74*)
	NEE_{dry}	2.81 (53.4, *0.72*)	0.015 (0.230, *0.74*)
VPRM-TRG	**NEE_{ann}**	0.402 (7.64, *0.77*)	-0.239 (3.73, *0.76*)
	NEE_{wet}	0.020 (0.373, *0.77*)	-1.48 (23.0, *0.76*)
	NEE_{dry}	0.456 (8.67, *0.77*)	-0.007 (0.103, *0.77*)
VPRM-SIF	**NEE_{ann}**	0.451 (8.57, *0.71*)	-0.326 (5.09, *0.77*)
	NEE_{wet}	0.064 (1.22, *0.71*)	-1.15 (17.9, *0.77*)
	NEE_{dry}	0.591 (11.2, *0.77*)	-0.021 (0.324, *0.77*)
VPRM-SIFg	**NEE_{ann}**	0.362 (6.88, *0.78*)	-0.173 (2.71, *0.78*)
	NEE_{wet}	0.146 (2.79, *0.78*)	-0.592 (9.24, *0.78*)
	NEE_{dry}	0.469 (8.92, 0.*78*)	-0.00 (0.013, *0.78*)

Figure S8 displays diurnal patterns in seasonal predictability. While the diurnal averaging by season smooths the hourly model-observation mismatch displayed in Table S4, the diurnal breakdown suggests improved respiration parameterization in the SIF-based VPRM formulations.

While Br-K67 seasonal predictions using annually fit parameters smoothed the impacts of lower cross-season predictability, the cross-season results (Table S4, Fig. S8) combined with the order-of-magnitude higher LUEs (Fig. S7a), indicate the traditional VPRM formulations are driven by environmental variables that inadequately represent the dominant land cover type in the study domain. The exceptionally poor VPRM-TRA results also brings into question the reliability of the VPRM-TRG formulation given that they both incorporate the same environmental predictors. We also note that across all model versions, model-observation mismatch was highest in the wet season which is intuitive given the added complexity of cloud cover and associated impacts on uncertainties in remotely sensed environmental drivers and light use efficiency.